INTEGRATED GPS RECEIVER FOR REMOTE SENSING SEA STATE AND LAND COVER

Lie Chung Shen[1], Jhy Ching Juang[2], Ping Ya Ko[3], Ching Lang Tsai[1] and Ching Liang Tseng[1]

1. Earth Research and Science Academy, National Cheng Kung University, Taiwan; shens.art(at)msa.hinet.net
2. Electrical Engineering Academy, National Cheng Kung University, Taiwan
3. General Director of Material and Electro-optical Division, CSIST, Taiwan

ABSTRACT

In this paper, a new application and the development of a highly integrated GPS receiver that uses reflected GPS signals for ground object detection and Digital Terrain Elevation Data (DTED) mapping are described. First, both right-hand circular polarisation (RHCP) and left-hand circular polarisation (LHCP) antennas are employed so that direct and reflected signals can be acquired simultaneously. The direction of arrival of the signals may be along the reflected signal path or along the line of sight of a particular satellite. The aim of this study is to exploit the carrier phase, reflectivity of L1/L2 signal-to-noise density ratio components of the reflected signals, and direct signals for fresh stream water, ocean water, and ground object detection. The sea states are predicted by using the Doppler shifts resulting from the surface reflection from a moving surface. An integer ambiguity algorithm is also implemented. During the development and test stage, the DTED and satellite images are used and mapped using the integrated software.

Keywords: Reflection coefficient, object detection, sea surface, terrain mapping, global positioning system

INTRODUCTION

A reflected GPS signal contains information on the reflecting object since the characteristics of the reflected signal vary substantially depending on the reflecting object. In this paper, a new application and the development of a highly integrated GPS receiver that uses reflected GPS signals for ground object detection and visual element function mapping are described. Several application considerations have been analysed in order to successfully acquire and track weak, reflected GPS signals from the ground surface. First, both RHCP and LHCP antennas are employed so that direct and reflected signals can be acquired simultaneously. The direction of arrival of the signals may be along the reflected signal path or even along the line of sight of a particular satellite. Unlike most existing GPS reflection experiments, the aim of this study is to exploit the carrier phase and reflectivity of L1/L2 *SNR* components of the reflected signals and direct signals for the detection of stream calm water, disturbed water, and bare soil (1). A stream flow is predicted by using the Doppler shifts resulting from the surface reflection from the moving surface. Rough sea states and wind speeds are estimated by using the time delay in ocean-scattered signals and Doppler shifts. The terrain moisture classes and the visual element terrain are defined by using two GPS-derived reflectivity classification features and land-cover classes containing a surface/soil moisture component, respectively. An integer ambiguity algorithm has also been implemented. During the development and test stages, DTED level 2 (~30 m pixel accuracy) and visual elements of satellite images (~2.0 m pixel accuracy) have been used and mapped using the integrated software (2). For the remote sensing of oceans, landscapes, and streams, the accuracy of each reflection altitude is between 10 cm and 30 cm. The accuracy of each reflection area is between 2 cm and 10 cm.

ALGORITHM DESCRIPTION

In this section, algorithms for the processing of direct and reflected dual-frequency GPS signals are delineated. The integrated GPS receiver system utilises two antennas, RHCP and LHCP an-

tennas, to receive direct and reflected GPS signals at two frequencies L1 and L2. At any measurement epoch, when all the signals are available, there are eight measurements in total. These measurements are pre-processed so that outliers are removed and used for the determination of the position of the two antennas at the bridge. The height of the bridge is 13.2 m (from the bridge floor to the bridge pier). The altitude of the bridge floor is 446.25 m with regard to the ground sea level. Consequently, information pertaining to the water level of the stream, stream flow, and ground reflective index can be obtained. Figure 1 depicts a typical experimental setup in which a 6.5-m boom is extended from a base so that the two antennas are placed above a stream. The three LHCP antennas are placed orthogonally on the stream surface so that the reflected signals from different directions can be observed. In contrast, only one RHCP antenna is used to receive direct GPS signals.

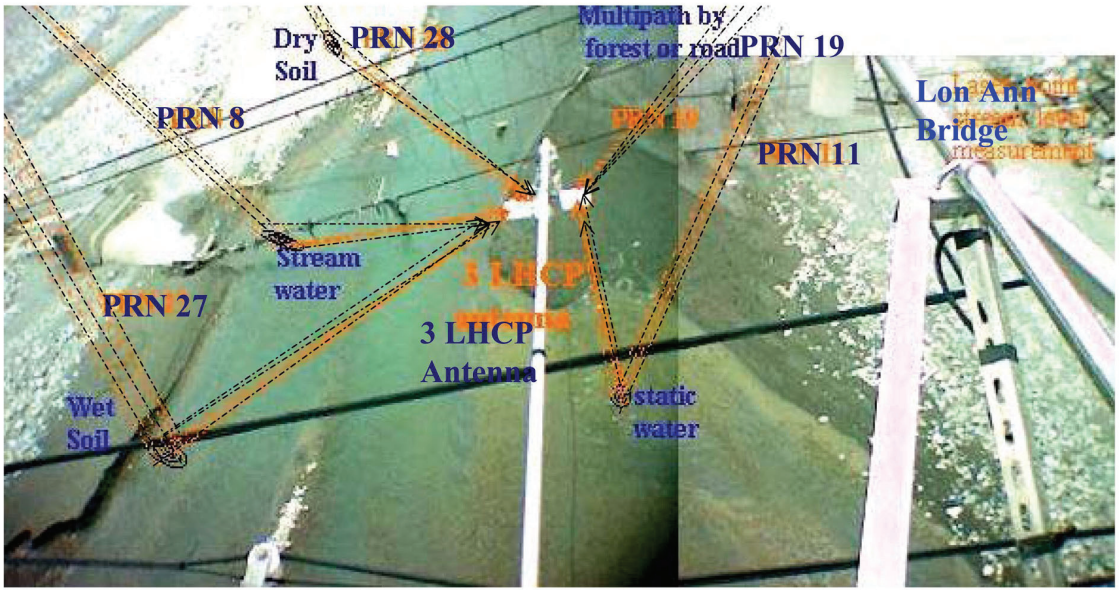

Figure 1: Antenna setup during data collection at Lon Ann Bridge.

GPS Measurements

The GPS signals being broadcast from orbiting satellites may be reflected from a water body or the ground surface. Since the direct line-of-sight signals are right-hand circular polarised, the reflected signals introduce left-hand circular polarisation. The reflected signals can then be better received by an LHCP antenna. The direct line-of-sight signal can be represented as (3)

$$X_d(t) = g\left(t - \frac{r_d(t)}{c} - \frac{k}{f_c^2}\right) \cdot \exp\left(j2\pi f_c\left(t - \frac{r_d(t)}{c} + \frac{k}{f_c^2}\right)\right) \tag{1}$$

where $g(\bullet)$ is the code, f_c the carrier frequency, $r_d(t)$ the distance between the receiving antenna and the satellite, and k/f_c^2 the ionospheric delay. After reflection, the signal becomes

$$X_r(t) = \int F(P)\sqrt{\sigma(P)}\, g\left(t - \frac{r_r(P,t)}{c} - \frac{k}{f_c^2}\right) \cdot \exp\left(-j2\pi f_c\left(t - \frac{r_r(P,t)}{c} + \frac{k}{f_c^2}\right)\right) \mathrm{d}A(P) \tag{2}$$

where P is the reflection point on the surface, $F(P)$ the voltage gain of the receiving antenna in the direction of the reflection point, $\sigma(P)$ the bistatic radar cross section, $r_r(P,t)$ the geometric path length of the ray scattered from P, and $\mathrm{d}A(P)$ a small element of area centred at P. By comparing the two Eqs. (1) and (2), it is evident that the reflected signals carry information pertaining to the reflection surface.

For a dual-frequency GPS receiver, both code and phase measurements can be used to determine the time, position, and relevant parameters such as ionospheric delays. In addition, when measurements from two antennas with different polarisations (RHCP and LHCP antennas) can be obtained (4), the terrain information can be extracted. GPS satellites broadcast signals at L1 and L2 frequencies. Let f_1 and f_2 and λ_1 and λ_2 be the frequencies and wavelengths of L1 and L2, respectively. It is known that dual frequency measurements can be used to effectively remove ionospheric delays. The code and phase measurements at the two frequencies can be expressed as (5)

$$P_{1s} = R_s + c\left(\mathrm{d}t - \mathrm{d}T\right)_s - I + T + \varepsilon_{p1s} \tag{3}$$

$$\Phi_{1s} = R_s + c\left(\mathrm{d}t - \mathrm{d}T\right)_s - I + T + \lambda_1 N_{1s} + \varepsilon_{\phi 1s} \tag{4}$$

$$P_{2s} = R_s + c\left(\mathrm{d}t - \mathrm{d}T\right)_s + (f_1/f_2)^2 I + T + \varepsilon_{p2s} \tag{5}$$

$$\Phi_{2s} = R_s + c\left(\mathrm{d}t - \mathrm{d}T\right)_s - (f_1/f_2)^2 I + T + \lambda_2 N_{2s} + \varepsilon_{\phi 2s} \tag{6}$$

where P_{1s} and P_{2s} and Φ_{1s} and Φ_{2s} are the code and phase at the L1 and L2 frequencies, respectively. The subscript *s* is used to represent either the direct (*d*) signal or the reflected (*r*) signal. The terms on the right-hand sides of Eqs. (3)-(6) can be explained as follows: R_s is the distance between the satellite and the observation point, $c(\mathrm{d}t\text{-}\mathrm{d}T)_s$ is the satellite clock time delay, I the ionospheric delay at the L1 frequency, T the tropospheric delay, N_{1s} the integer ambiguity at the L1 frequency, and N_{2s} the L2 integer ambiguity. The remaining terms ε_{p1s}, $\varepsilon_{\phi 1s}$, ε_{p2s} and $\varepsilon_{\phi 2s}$ represent noise.

When the dual-frequency code and phase measurements are available, one can employ estimation techniques to estimate the position, clock offset, integer ambiguities, and ionospheric/tropospheric delays. The act estimation can be performed in an iterative manner, especially when measurements from the LHCP and RHCP antennas are used.

The software used for the processing of reflected GPS signals determines the antenna position through carrier phase measurement processing with integer ambiguity resolution, calculation of the reflection point through the use of the digital terrain elevation database and multispectral satellite images, estimation of the reflectivity of a ground object, and estimation of a stream flow through Doppler frequency shift. The procedure for the processing comprises the following steps:

1. Determination of the antenna position. Typically, a GPS receiver gives a position estimate of the antenna in the range of several meters. Using carrier phase measurements and integer ambiguity techniques, the position of the antenna can be estimated with an accuracy of several decimetres (6). In the software, an altitude iteration loop is also used so that the accuracy is further improved.
2. Compensation for ionospheric and tropospheric errors. Since dual frequency receivers are used, processing the dual frequency measurements can compensate for ionospheric errors. The tropospheric error is corrected using a tropospheric delay model.
3. Estimation of the reflection point. The reflection point depends on the path of signal propagation. As the positions of the antenna and satellite can be computed, the reflection point is constrained to the plane established by the two positions and the geo-centre. In the determination of the reflection point, special care is exercised to estimate the altitude as one of the objectives is to estimate the ground object height through the processing of reflected signals. To this end, the digital terrain elevation database is used so that the measurements are correlated with the existing model.
4. Estimation of reflectivity. When the attenuated reflected signal is compared with the direct signal, information pertaining to the properties of the ground object is obtained. The signal strengths of the direct and reflected signals are processed to estimate the reflectivity in this step. Multispectral satellite images around the reflection area are also used so that the measurements can be compared with the existing data model.

5. Estimation of stream flow. When the reflection points are located on the surface of a stream, the computed reflection points are subject to variations in Doppler shifts of the stream. Such information is examined to estimate the speed and direction of the stream flow.

In the following, the algorithms for the determination of the reflection point, reflectivity, and stream flow are described. Essentially, the reflection point is determined by comparing the time delay between the direct and the reflected signals. In contrast, the reflectivity is estimated by comparing the signal-to-noise ratios between the direct and the reflected signals. Furthermore, the stream flow is estimated by studying the Doppler variation of the reflected signals.

Determination of Reflection Point

In order to extract stream flow information from the reflected signal, it is essential to obtain the coordinates of the reflection point. As illustrated in Figure 2, the reflection point can be computed when the positions of the satellite and receiver are known. The LHCP antenna position (*Lon*, *Lat*, $H^{ti})_{LHCP}$ transforms to (X_r,Y_r,Z_r) (*ti*: instantaneous number of satellites for LHCP receiver), and satellite position (*Lon*, *Lat*, $H)^i$ transforms to (X^i_s,Y^i_s,Z^i_s) (*i*: ID of satellite).

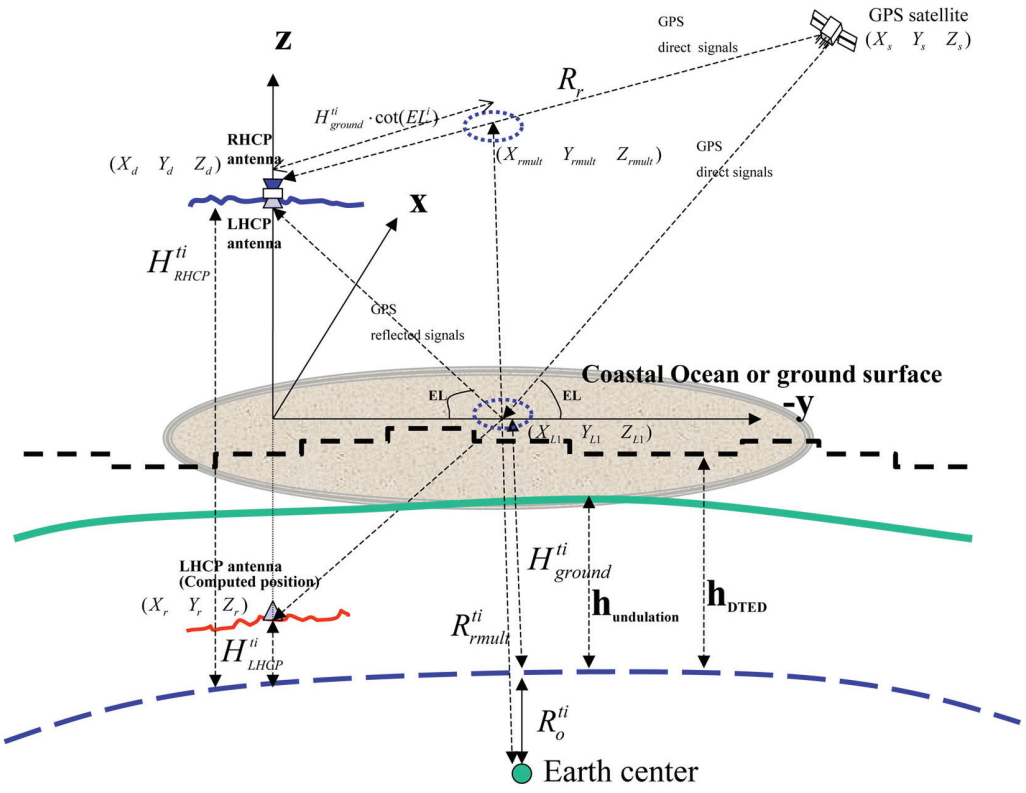

Figure 2: The mean ground altitude profile.

The altitude of ground or water surface is given by Eq. (7) (7). Since the projection of the reflected point on line of sight is (*Lon*, *Lat*, $H)^{ti}$, the coordinate on the ground transforms to (X_g,Y_g,Z_g). Eq. (8) used the radius of the ground for receiver position R^{ti}_o and the reflected multi-pole point $(X_{rmult},Y_{rmult},Z_{rmult})^l$ is derived by the satellite position using the satellite's elevation angle and RHCP position.

$$H^i_{ground} = \frac{(H^i_{RHCP} + H^{ti}_{LHCP})}{2} \tag{7}$$

$$\begin{bmatrix} X_{rmult} \\ Y_{rmult} \\ Z_{rmult} \end{bmatrix}^{i} = \left[\frac{\left[R_r - H^{i}_{ground} \cdot \cot\left(EL^{i} \right) \right]}{R_r} \right] \cdot \begin{bmatrix} X_d - X^{i}_{s} \\ X_d - X^{i}_{s} \\ X_d - X^{i}_{s} \end{bmatrix} + \begin{bmatrix} X_s \\ Y_s \\ Z_s \end{bmatrix}^{i} \tag{8}$$

R^{ti}_{mult} is the radius of the reflected multi-pole point between the reflection position and the line of sight; Eq. (9) for R_{rmult} was obtained from Eq. (8). Eqs. (7), (8), and (9) give Eq. (10). The reflection point centre is represented by (X_{L1}, Y_{L1}, Z_{L1}) and the elevation angle of the satellite by EL^{i}.

$$R^{i}_{rmult} = \left\{ \left(X_{rmult} \right)^2 + \left(Y_{rmult} \right)^2 + \left(Z_{rmult} \right)^2 \right\}^{0.5} \tag{9}$$

$$\begin{bmatrix} X_{L1} \\ Y_{L1} \\ Z_{L1} \end{bmatrix}^{ti} = \frac{R^{ti}_{o}}{R^{i}_{rmult}} \cdot \begin{bmatrix} X_{rmult} \\ Y_{rmult} \\ Z_{rmult} \end{bmatrix}^{i} \tag{10}$$

An alternative is to use suitable relative heights. The authors use GPS data for H^{i}_{RHCP} and H^{ti}_{LHCP} for the subtraction as well as the Digital Terrain Elevation Data (DTED) level 2 (~90 ft pixel) mapping with $h_{undulation}$. The value of $h_{undulation}$ is provided from the output of the GPS solution tool in the GPS receiver to the notebook (control log command: BESTPOSITION). Hence, the ground or water surface altitude of Taiwan's local height is given by Eq. (11) as follows:

$$\begin{aligned} H^{i}_{RHCP} &= H^{i}_{RHCP} - h_{undulation} \\ H^{ti}_{LHCP} &= H^{ti}_{LHCP} - h_{undulation} \\ H^{ti}_{ground} &= \frac{(H^{i}_{RHCP} + H^{ti}_{LHCP})}{2} - h_{undulation} \end{aligned} \tag{11}$$

Object Detection and Reflectivity

The reflection or scattering of the GPS signal by an object depends on the surface roughness and electrical properties (conductivity and permittivity) of the reflecting material. In fact, different materials such as dry ground (grass), wet ground (different compositions of sand, silt, and clay), tree, forest, fresh stream water, ocean water body, road, and concrete may provide different reflectivities (8). The surface reflectivity $\Re$, which is defined as the ratio of the reflected power to the direct power, can be used for the classification of ground objects. Dinesh Manandhar (9) showed that the resultant reflection coefficient is the sum of the co-polar and cross-polar reflection coefficients. Since GPS signals are circularly polarised, the reflection coefficient is actually a function of the elevation angle from the receiver to the satellite. This coefficient is denoted as F_c and it can be computed once the elevation angle is known. The surface reflectivity $\Re^{i}_{s}$ is related to the reflection coefficient and the relative signal-to-noise ratios between the reflected and direct signals. More precisely,

$$\Re^{i}_{s} = F_c(EL^{i}_{s} \quad C^{ti}_{s}) \cdot \frac{SNR^{i}_{rs}}{SNR^{i}_{d}} \tag{12}$$

where SNR^{i}_{rs} and SNR^{i}_{d} are the signal-to-noise ratios of the reflected and direct signals, respectively. $F_c(EL^{i}_{s} \quad C^{ti}_{s})$ is the reflection coefficient factor for the reflecting surface and it depends on the ground surface object and the propagation angle of the GPS signals. In this study, both L1 and L2 GPS signals are used and hence the reflectivity at the two frequencies can be separately computed. Since the image around the observation area can be obtained, a database is constructed based on multispectral data for the classification of the ground object. Consequently, the reflectivity

computed on the basis of the measured data can be correlated with the existing database for the purpose of training/tuning the system parameters and for object classification. An apparent advantage of using the multispectral database is that the reflection point (whether it be a water surface or a tree) can be identified.

Variation of Doppler and Stream Flow

When the reflection point can be determined and the ground object can be identified at each epoch, the stream flow velocity can be roughly estimated by computing the variation of the reflection point as a function of time and processing the Doppler measurements. This situation is depicted in Figure 3. The Lorentz transformation Λ is given by Eq. (13). This equation has been used to relate the wave four-vectors between the incoming wave and the reflected wave (10). A similar approach is adopted for the determination of the stream flow.

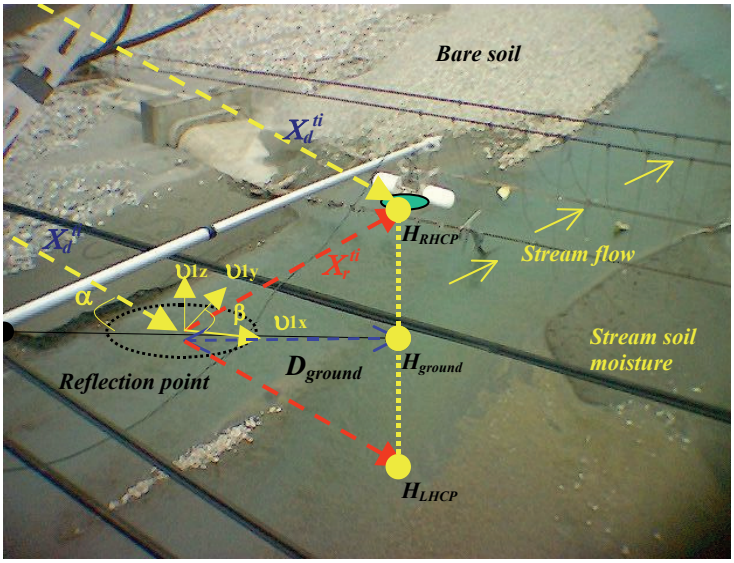

Figure 3: Reflection from a moving surface such as a stream flow, which is determined using the RHCP receiver position.

$$\Lambda \equiv \begin{bmatrix} \gamma & -\gamma\frac{v_x}{c} & -\gamma\frac{v_y}{c} & -\gamma\frac{v_z}{c} \\ -\gamma\frac{v_x}{c} & 1+\eta\frac{v_x^2}{v^2} & \eta\frac{v_x v_y}{v^2} & \eta\frac{v_x v_z}{v^2} \\ -\gamma\frac{v_y}{c} & \eta\frac{v_x v_y}{v^2} & 1+\eta\frac{v_y^2}{v^2} & \eta\frac{v_y v_z}{v^2} \\ -\gamma\frac{v_z}{c} & \eta\frac{v_x v_z}{v^2} & \eta\frac{v_y v_z}{v^2} & 1+\eta\frac{v_z^2}{v^2} \end{bmatrix} \tag{13}$$

We consider a frame centred at the reflection point; the *z*-axis is perpendicular to the surface, the *x*-axis is toward the receiver, and the *y*-axis is obtained by the right-hand rule. We assume that the flow velocity vector in this frame is

$$\boldsymbol{v} = \begin{bmatrix} v_x \\ v_y \\ v_z \end{bmatrix}$$

and the speed is $v = \sqrt{v_x^2 + v_y^2 + v_z^2}$. The wave four-vector of the incoming signal is denoted by

$$\begin{bmatrix} 2\pi f_d / c \\ k_x \\ k_y \\ k_z \end{bmatrix},$$

where f_d is the Doppler frequency and c is the speed of light. According to Snell's law, the Doppler frequency of the reflected signal is related to the Doppler frequency of the direct signal and the flow velocity by the following formula:

$$X_r^{ti} \equiv \begin{bmatrix} 2\pi f_r / c \\ k_{xr} \\ k_{yr} \\ k_{zr} \end{bmatrix} \equiv \Lambda^{-1}\Lambda X_d^{ti} \equiv \begin{bmatrix} \left(\gamma^2 + \frac{v^2}{c^2}\right) & \frac{-2\gamma^2}{c}v_x & \frac{-2\gamma^2}{c}v_y & \frac{-2\gamma^2}{c}v_z \\ NA & NA & NA & NA \\ NA & NA & NA & NA \\ NA & NA & NA & NA \end{bmatrix} \cdot \begin{bmatrix} 2\pi f_d / c \\ k_{xd} \\ k_{yd} \\ k_{zd} \end{bmatrix}^{ti}$$

$$\begin{bmatrix} 2\pi f_r / c \\ k_{xr} \\ k_{yr} \\ k_{zr} \end{bmatrix} \equiv \begin{bmatrix} \frac{2\pi f_d}{c}(2\gamma^2 - 1) - 2\gamma^2 \frac{v_x}{c}k_{xd} - 2\gamma^2 \frac{v_y}{c}k_{yd} - 2\gamma^2 \frac{v_z}{c}k_{zd} \\ -\frac{2\pi f_d}{c}\frac{v_x}{c}2\gamma^2 + \left(1 + 2\frac{v_x^2\gamma^2}{c^2}\right)k_{xd} + v_x v_y\left(2\frac{\gamma^2}{c^2}\right)k_{yd} + v_x v_z\left(2\frac{\gamma^2}{c^2}\right)k_{zd} \\ -\frac{2\pi f_d}{c}\frac{v_y}{c}2\gamma^2 + v_x v_y\left(2\frac{\gamma^2}{c^2}\right)k_{xd} + \left(1 + 2\frac{v_y^2\gamma^2}{c^2}\right)k_{yd} + v_y v_z\left(2\frac{\gamma^2}{c^2}\right)k_{zd} \\ -\frac{2\pi f_d}{c}\frac{v_z}{c}2\gamma^2 + v_x v_z\left(2\frac{\gamma^2}{c^2}\right)k_{xd} + v_y v_z\left(2\frac{\gamma^2}{c^2}\right)k_{yd} + \left(1 + 2\frac{v_z^2\gamma^2}{c^2}\right)k_{zd} \end{bmatrix} \quad (14)$$

$$f_r = \left(\frac{c^2}{c^2 - v^2} + \frac{v^2}{c^2}\right)f_d - \frac{v_x}{\pi}\gamma^2 k_x - \frac{v_y}{\pi}\gamma^2 k_y - \frac{v_z}{\pi}\gamma^2 k_z$$

where f_γ is the Doppler frequency of the reflected signal and

$$\gamma = \sqrt{\frac{1}{1 - v^2/c^2}}.$$

We determine α as the elevation angle and β be the angle between the flow direction and the *x*-axis in the plane. From the figure, the three terms $\gamma^2 k_x/\pi$, $\gamma^2 k_y/\pi$, and $\gamma^2 k_z/\pi$ can be approximated, respectively, as

$$\begin{aligned} \frac{\gamma^2}{\pi}k_x &\cong \frac{\gamma^2}{\pi}\cdot 2\frac{\pi}{\lambda}\cos(\alpha)\cos^2(\beta) \approx \frac{2}{\lambda}\cos(\alpha)\cos^2(\beta) \\ \frac{\gamma^2}{\pi}k_y &\cong \frac{\gamma^2}{\pi}\cdot 2\frac{\pi}{\lambda}\cos(\alpha)\sin^2(\beta) \approx \frac{2}{\lambda}\cos(\alpha)\sin^2(\beta) \\ \frac{\gamma^2}{\pi}k_z &\cong \frac{\gamma^2}{\pi}\cdot 2\frac{\pi}{\lambda}\sin(\alpha) \approx \frac{2}{\lambda}\sin(\alpha) \end{aligned} \quad (15)$$

where λ is the wavelength. Hence, the Doppler frequency of the reflected signal becomes

$$f_r = f_d - \frac{2v_x}{\lambda}\cos(\alpha)\cos^2(\beta) - \frac{2v_y}{\lambda}\cos(\alpha)\sin^2(\beta) - \frac{2v_z}{\lambda}\sin(\alpha) \tag{16}$$

The two angles can also be approximated by (11)

$$\sin(\alpha) \approx \delta(h_{ground})/d_{ground}$$

$$\cos(\alpha) \approx \delta(h_{RHCP} - h_{ground})/d_{ground}$$

$$\sin(\beta) \approx \delta(d_{ground})/d_{ground}$$

$$\cos(\beta) \approx \left(d_{ground} - \delta(d_{ground})\right)/d_{ground}\ .$$

Within a time interval, the reflection angle changes by

$$\delta(\sin(\alpha)) \approx (\delta(\alpha))^{ti}$$

$$\delta(\sin(\beta)) \approx (\delta(\beta))^{ti}$$

and the frequency shift changes by

$$\delta(\Delta f)^{ti} / \delta(Time) \approx \left(\frac{f_{sr} - f_{sd}}{1.0}\right)^{ti}$$

according to Eq. (17), and thus:

$$\frac{\delta(\Delta f)^{ti}}{\delta(Time)} \cong \left(\frac{f_{sr} - f_{sd}}{1.0}\right)^{ti} \approx \frac{-2}{\lambda_s}\left(v_x\cos(\alpha)\cos^2(\beta) + v_y\cos(\alpha)\sin^2(\beta) + v_z\sin(\alpha)\right) \tag{17}$$

$$\frac{\delta(\Delta f)^{ti}}{\delta(H_{ground})} \cong -\frac{2}{\lambda}\frac{v_z}{D_{ground}}\delta(Time) \approx -\frac{2}{\lambda}\frac{V_{SAT}}{R_{ground}}\delta(Time) \cong -\frac{2}{0.00019}\cdot\frac{4.6\ \text{km/s}}{22000\ \text{km}}\cdot 1.0$$

$\frac{\delta(\Delta f)^{ti}}{\delta(H_{ground})} \cong 2.5$ Hz/km $= \frac{1}{400}$Hz/m , for the present case $\frac{\delta(\Delta f)^{ti}}{\delta(H_{ground})} \cong (3.5 - 8.0)$ Hz/km

The velocity of the stream flow is obtained from the wavelength of the L1 or L2 band frequency, the Doppler shifts $\delta(\Delta f)^{ti}/1000 \approx$ Hz/km of the reflected and direct signals, the reflection angle, and the relative distance and altitude of the reflection points. Eqs. (16) and (17) give Eq. (18). The reflection angle α changes by $\delta\alpha \equiv D^{ti}_{ground}/\delta\left(H_{ground}\right)$ with the distance D^{i}_{ground} between the reflection point and the RHCP receiver position. The stream flow vector angle β changes by $\delta\beta \equiv D^{ti}_{ground}/\delta\left(D_{ground}\right)$ when $\delta\left(D^{i}_{ground}\right)$ depends on the satellite and reflection points.

$$\vec{v}_1 \equiv \begin{pmatrix} v_{1x} \\ v_{1y} \\ v_{1z} \end{pmatrix}^{ti} \cong \begin{bmatrix} \frac{\lambda_1}{2}\cdot\frac{\delta(\Delta f)^{ti}}{1000}\cdot\frac{D^{ti}_{ground}}{\delta\left(H_{RHCP} - H_{ground}\right)}\left(\frac{D^{ti}_{ground}}{\delta\left(D_{ground}\right)}\right)^2 \\ \frac{\lambda_1}{2}\cdot\frac{\delta(\Delta f)^{ti}}{1000}\cdot\frac{D^{ti}_{ground}}{\delta\left(H_{RHCP} - H_{ground}\right)}\frac{\left(D^{ti}_{ground}\right)^2}{D^2_{ground} - \delta\left(D_{ground}\right)^2} \\ \frac{\lambda_1}{2}\cdot\frac{\delta(\Delta f)^{ti}}{1000}\cdot\frac{D^{ti}_{ground}}{\delta\left(H_{ground}\right)} \end{bmatrix} \tag{18}$$

EXPERIMENTAL RESULTS

In the data collection campaign, a specially designed antenna is used so that both direct RHCP and reflected LHCP GPS signals can be received. The RHCP antenna (NovAtel GPS-700) is used to ensure the quality of GPS signals as well as to provide correction information for the processing of the reflected signals. The LHCP antennas (H601) are used to collect the reflected signals and consequently to derive remote sensing related information. In fact, three LHCP antennas are used. These three antennas are mounted perpendicular to each other so that signals reflected from different directions can be received. The incoming signals from different LHCP antennas are combined and received by a GPS receiver (SOKKIA 2600). The RHCP signal is received through another GPS receiver. Hence, at each epoch, dual-frequency and dual-polarised measurements are obtained. The processing tool is developed using MATLAB software. In addition, satellite imagery and the DTED around the experimental region are used to enhance the development of the processing tool and for the verification of the result. Figure 1 illustrates the antenna setup in the data collection campaign at Lon Ann Bridge near Tai-Chung, Taiwan. An aluminum bar of length 6.5 m is extended from the bridge over the stream. At the tip of the bar, the three LHCP antennas are mounted perpendicular to each other. The GPS signal traces are also plotted in the figure so that the collection of the reflected signals can be visualised. The RHCP antenna and receiver are installed on the bridge. Figure 4 illustrates the antenna setup in the data collection campaign at Wu-Chi pier near Tai-Chung Port; the three LHCP antennas on the aluminum bar are extended from the Pier over the ocean area. The RHCP antenna and receiver are installed on the pier.

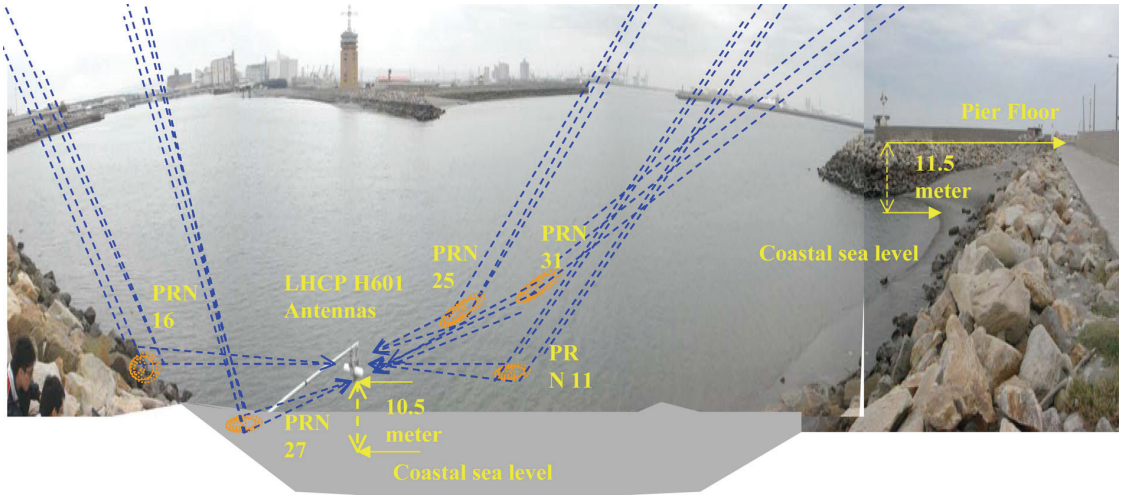

Figure 4: Three LHCP antennas mounted on an aluminium bar are extended over the ocean area at Wu-Chi pier.

Determination of Reflection Points

The locations of the RHCP and LHCP antennas can be determined by using the GPS measurement data. Typically, the receiver would provide a float position and the computed position would be obtained from a fixed ambiguity solution method. The data were collected on November 2, 2006 from (UTC time) 06:07:56 to 07:25:56 around Da-Ga River near Tai-Chung, Taiwan. The results of a comparison between a high-resolution (~50 cm pixels) satellite image and a DTED resolution (~30 m pixels) raster image are shown in Figure 5. The location of the LHCP antenna is determined to be at longitude 120.8373°E, latitude 24.17211°N, and altitude 419.282 m. In contrast, the positions of the LHCP/RHCP antennas are LHCP fixed position (24.17211°N, 120.8373°E, 419.282 m) and RHCP fixed position (24.17182°N, 120.83732°E, 446.682 m). With regard to the reflection points, the satellite signals PRN 8, 11, 27, and 28 are reflected from the stream and the satellite signal PRN 19 is reflected from the ground. The altitudes of the reflection points on the stream are 434.126 m, 434.083 m, 434.147 m, and 434.160 m. The altitude of the reflection point on the ground for PRN 19 is 455.195 m.

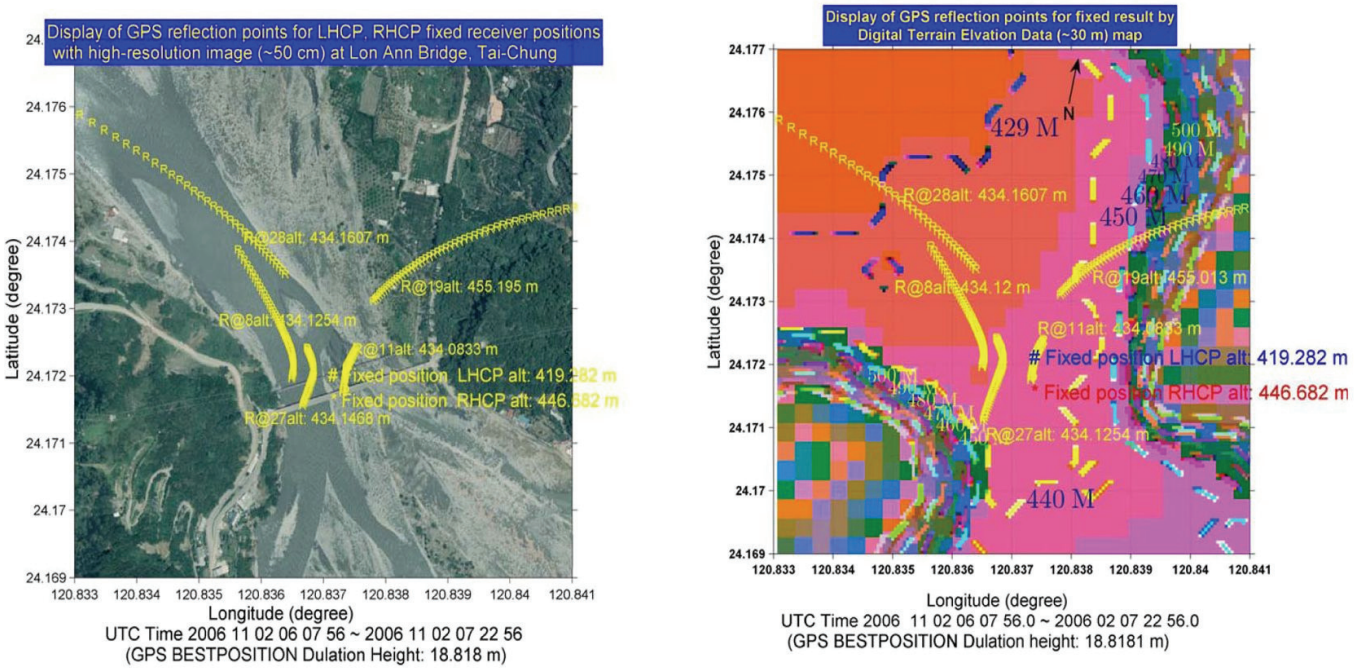

Figure 5: Comparison analyses of satellite image and DTED raster image for the reflection area and receiver positions on Lon Ann Bridge along with altitude estimation.

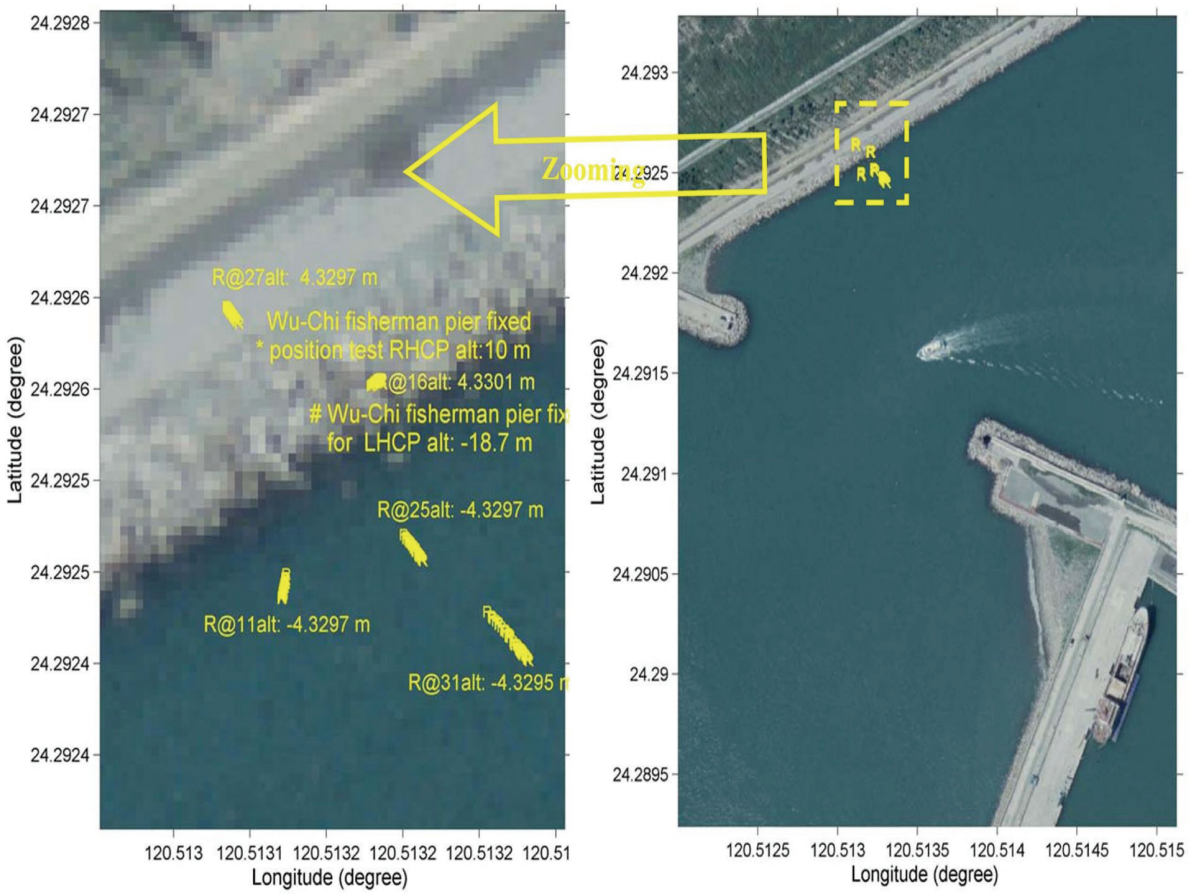

Figure 6: Reflected area and receiver positions with altitude estimation on Wu-Chi Pier (UTC Time 2006 11 14 03 39:01–03 54:02 UT (11:39–11:54 am LT)).

The GPS signal traces for another reflected GPS measurement are also plotted in Figure 6 so that the collection of reflected signals can be visualised. The reflection areas of calm sea water, disturbed sea water, a wave, and a concrete road on Wu-Chi Pier at Tai-Chung Port, Tai-Chung, are determined and described. The reflection area of the ocean and tides are determined and described.

The sea surface reflection points and high-resolution (~50 cm pixels) images for PRNs 11, 25, and 31 do not show reflection point trajectories similar to the trajectory of PRNs 16 and 27. The sea level of the ocean was determined to be between -4.329 m and -4.330 m from the reflection foot-prints at Wu-Chi Pier, Tai-Chung Port.

Classification of Object Detection and Reflectivity Analysis

Since the antenna height is approximately 13 m (between the bridge and the stream surface), the authors observed a reflected signal with an extra path length of approximately 250~300 m. The better results and measurements of the LHCP observations have been continuously locked and assigned by using the receiver's log command. The disturbed water surface R@27 (58.4°…61.3°) will provide specular reflection resulting in a reflected wave with a high amplitude as compared to the disturbed water surface R@8 (40.1°…48.0°) (shown in Figure 7). This difference may solve the problem of distinguishing between disturbed and calm waters. In fact, the disturbed water reflection area sometimes appears to give a zero GPS reflected signal for PRN 7. Further, none of the events studied are harmonic oscillation events (the disturbed water harmonic times are between 65 and 75 s). This is explained as follows: either the stream flow affects the harmonic time or the specific grazing angle modifies it at the reflection area. In these measurements, the reflection area for R@11 is on calm stream water. The authors believe that the R@11 reflection points are steady at high reflection elevation angles (76.7°…86.3°) and the R@19 reflection points are unsteady and reduce the reflected wave amplitude at low elevation angles (38.5°…31.4°) for a wet or dry ground surface or land with tree cover.

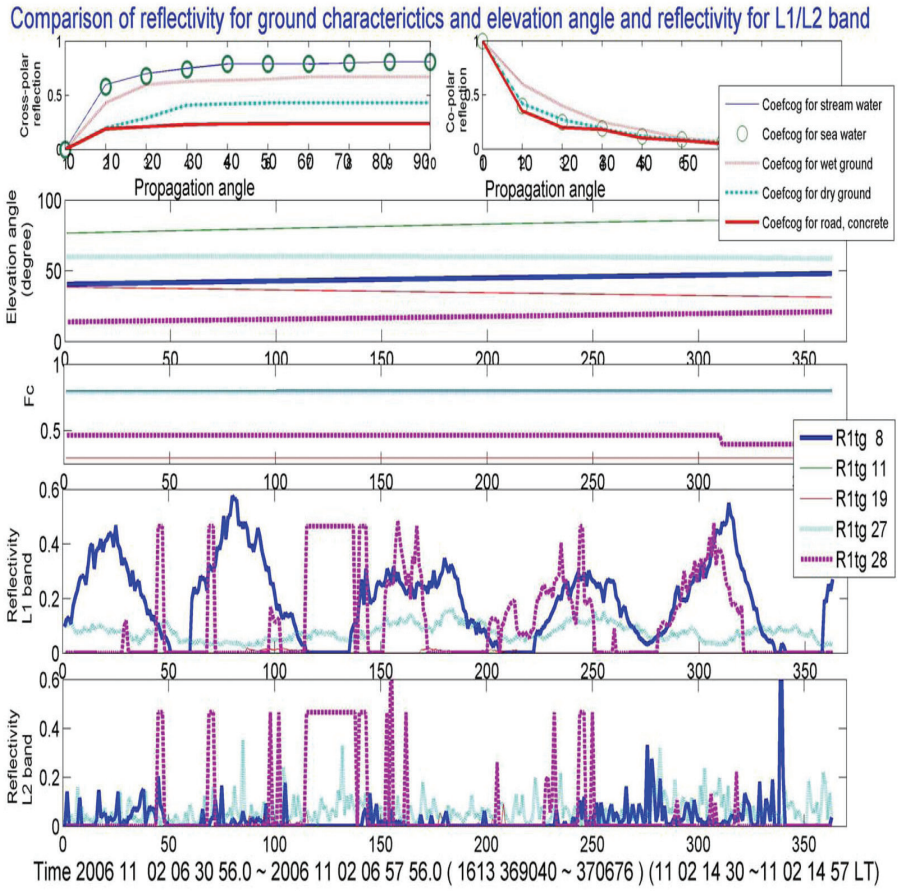

Figure 7: Comparison of L1/L2 reflectivity using satellite EL_s^{ti} angle and F_c scale for ground object.

Doppler and Stream Flow/Ocean State

Figure 8 shows the Doppler shifts of the satellite signals of PRNs 8, 11, and 27. It can be deduced that the flow speed around the corresponding reflection point is around 0.6270 m/s with a standard deviation of 0.7460 m/s, as shown in Figure 8. The three components of the flow velocity can be resolved, which gives the horizontal speed along the receiver direction as $v_x = 0.188 \pm 0.755$ m/s, horizontal velocity component perpendicular to the receiver direction as $v_y = 0.035 \pm 0.397$ m/s, and vertical component as $v_z = 0.080 \pm 0.424$ m/s.

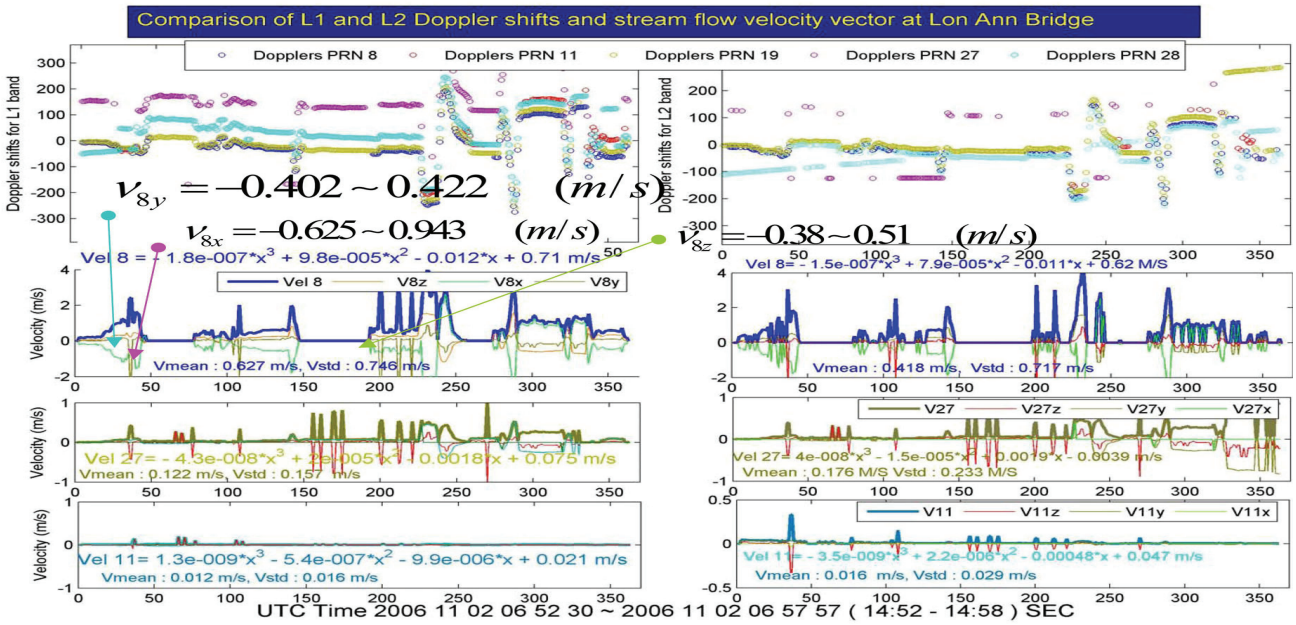

Figure 8: Comparison of stream flow velocity and Doppler shift at Lon Ann Bridge, Tai-Chung.

From a comparison of ocean tides by using Doppler shifts, sea surface reflection points, instantaneous rate of altitude H_{ground}, and range D_{ground}, the mean velocities of ocean tides are predicted to be in the range -6.954…+6.824 m/s (for PRN 31), -5.60…+5.64 m/s (for PRN 27), and -3.13…+3.07 m/s (for PRN 25) (Figure 9). Ocean tides and Doppler shifts for each reflected point are simulated and described using MATLAB.

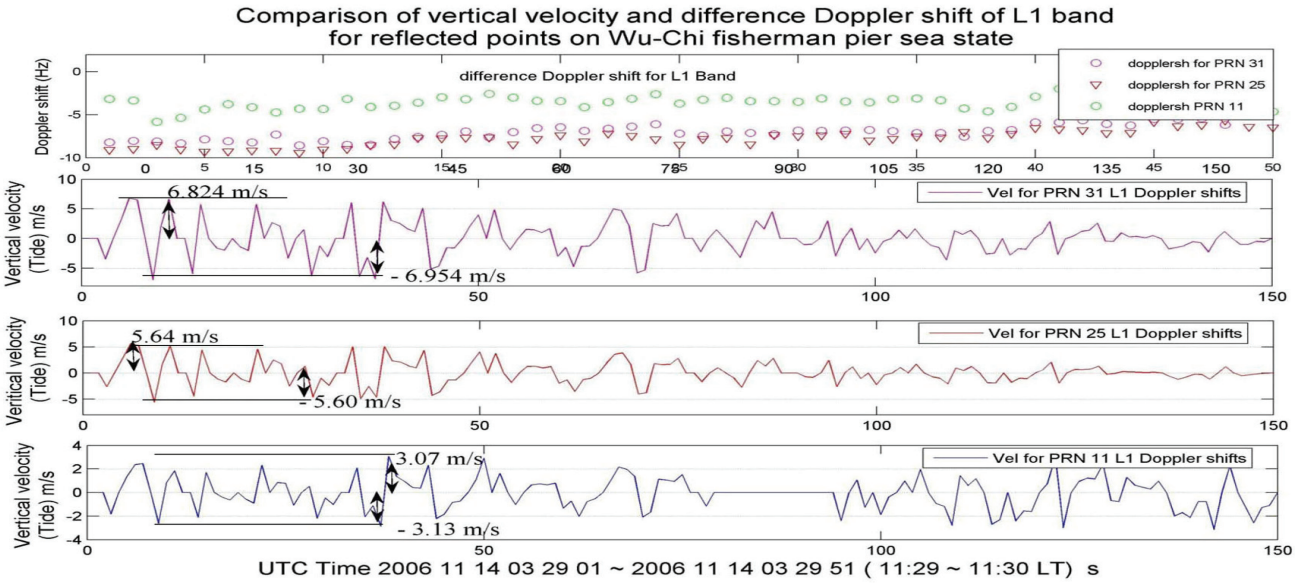

Figure 9: Comparison of stream flow velocity and Doppler shifts at Wu-Chi Pier, Tai-Chung Port.

CONCLUSIONS

This paper describes a GPS reflection experiment that is conducted to further explore the potential of GPS for remote sensing applications. Based on a dual-frequency, dual-polarisation setup, a set of direct and reflected GPS measurements are obtained. The carrier phase measurements are used to determine the reflection points. The results are then correlated with satellite images for the classification of the reflecting object and with digital terrain data to better quantify the data accuracy. An algorithm for stream flow determination is developed. The method is applied to analyse the stream flow along the Da-Gai River and the ocean tide at the location of Wu-Chi pier.

The classification of soil ground objects will be further improved upon by building a classification database using a reflected GPS signal analysis and measurement. The velocities of stream flow and ocean tides are estimated to be around 0.1-7.0 m/s by using Doppler shifts and a stream module. The authors would like to improve and remotely sense the soil classification of land cover for geodetic studies and topography determination. This study makes a significant contribution to GPS application and technology.

ACKNOWLEDGEMENTS

The authors would like to thank Dr. Yu (Satellite and Geodetic Research Center (SGRC), NCKU University, Taiwan) for providing the satellite images and DTED data. The authors would also like to thank Mr. Chen Houng-Shenq for his support in the measurements performed with the two receivers and three LHCP antennas. The authors express their thanks to Dr. Wickert for his advice and assistance in the modelling of tropospheric delay effects.

REFERENCES

1 Grant M S, S T Acton & S J Katzberg, 2007. Terrain moisture classification using GPS surface-reflected signals. IEEE Geoscience and Remote Sensing Letters, 4(1): 41-45

2 Weiss J P, P Axelrad & S Anderson, 2006. Assessment of Digital Terrain Models for multipath prediction at geodetic GNSS installations. ION GNSS 2006 Proceedings, 2815-2823

3 Ulaby F T, R K Moore & A K Fung, 1981. Microwave Remote Sensing, Active and Passive. Vol. 1 (Norwood, MA: Artech House)

4 Zavorotny V U & A G Voronovich, 2000. Scattering of GPS signals from the ocean with wind remote sensing application. IEEE Transactions on Geoscience and Remote Sensing, 38(2): 951-964

5 Goad C C & K Borre, 1996. RECPOS least-squares searching for receiver position for MATLAB. MATLAB Software Supply, 19 April 1996

6 Teunissen P J G, P J De Jonge & C C J M Tiberius, 1997. The least-squares ambiguity decorrelation adjustment: Its performance on short GPS baselines and short observation spans. Journal of Geodesy, 71(10): 589-602

7 Hajj G A & C Zuffada, 2003. Theoretical description of a bistatic system for ocean altimetry using the GPS signal. Radio Science, 38(5), 1089, doi:10.1029/2002RS002787

8 Kobayashi Y, K Sarabandi, L Pierce & M C Dobson, 2000. An evaluation of JPL TOPSAR for extracting tree heights. IEEE Transactions on Geoscience and Remote Sensing, 38(6): 2446-2454

9 Manandhar D, R Shibasaki & H Torioto, 2005. Prototype software-based receiver for remote sensing using reflected GPS signals. ION GNSS 2006 Proceedings, 643-652

10 Møller C, 1983. The Theory of Relativity (Oxford, UK: Clarendon)

11 Beyerle G, K Hocke, J Wickert, T Schmidt & C Reigber, 2002. GPS radio occultations with CHAMP: A radio holographic analysis of GPS signal propagation in the troposphere and surface reflections. Journal of Geophysical Research, 107(D24), 4802, doi:10.1029/2001JD001402